

Article

Characterization of a Nickel Sulfide Concentrate and Its Implications on Pentlandite Beneficiation

Linda D. Ayedzi ^{1,*}, Massimiliano Zanin ^{1,2}, William Skinner ¹ and George B. Abaka-Wood ^{1,*}

¹ ARC Centre of Excellence for Enabling Eco-Efficient Beneficiation of Minerals, Future Industries Institute, University of South Australia, Mawson Lakes Campus, Adelaide, SA 5095, Australia; max.zanin@mzminerals.com (M.Z.); william.skinner@unisa.edu.au (W.S.)

² MZ Minerals, Mineral Processing Consulting, Adelaide, SA 5082, Australia

* Correspondence: linda.ayedzi@mymail.unisa.edu.au (L.D.A.); george.abaka-wood@unisa.edu.au (G.B.A.-W.)

Abstract: In anticipation of future demands, a comprehensive understanding of the chemical and mineralogical characteristics of nickel-bearing minerals is a prerequisite to devising effective nickel beneficiation methods. Of particular importance are markers in the mineralogy of the flotation concentrate that inform beneficiation strategies to improve concentrate grades, increasing both the marketability and cost of refining. In this work, a detailed characterization of a complex nickel sulfide flotation concentrate from a Western Australian deposit was carried out to determine the mode of occurrence and distribution of nickel and the associated gangue minerals, with the view of identifying prudent beneficiation strategies to improve concentrate grades. The concentrate was characterized via particle, chemical, and mineralogical techniques. Particle size analysis of the concentrate showed that it consisted predominantly of fine and ultra-fine particles (<20 μm), with the nickel value concentrated in the finer size fractions. Nickel mineralization in the ore (by quantitative X-ray diffraction) was found to be within pentlandite, violarite, millerite, and gersdorffite. The sulfide gangue was predominantly pyrrhotite, pyrite, chalcopyrite, sphalerite, arsenopyrite, and galena. Quantitative evaluation of minerals by scanning microscopy (QEMSCAN) analysis revealed that nickel minerals are at least 91% liberated, and the remaining portion (around 7%) is locked within binary iron (Fe) sulfides and 2% within complex minerals. Based on these findings, potential processing options, such as magnetic separation, gravity separation, and froth flotation, for recovering and upgrading nickel from this concentrate are discussed. Notably, with the significant presence of ultrafine/fine pyrrhotite content, averaging around 52% in the minus 38 μm fraction, novel flotation cells, including the Jameson cell, column flotation cells, and Reflux flotation cell (RFC), have been identified as potential candidates for fine/ultrafine pentlandite recovery. Overall, the characterization study conducted suggests that acquiring knowledge about the mineralogical characteristics of existing mineral concentrates can serve as a pathway to improving future concentrate grades.

Keywords: nickel; pentlandite; pyrrhotite; particle size; liberation; ore characterization



Citation: Ayedzi, L.D.; Zanin, M.; Skinner, W.; Abaka-Wood, G.B. Characterization of a Nickel Sulfide Concentrate and Its Implications on Pentlandite Beneficiation. *Minerals* **2024**, *14*, 414. <https://doi.org/10.3390/min14040414>

Academic Editors: Sofia Barbosa and José António de Almeida

Received: 12 March 2024

Revised: 13 April 2024

Accepted: 16 April 2024

Published: 18 April 2024



Copyright: © 2024 by the authors. Licensee MDPI, Basel, Switzerland. This article is an open access article distributed under the terms and conditions of the Creative Commons Attribution (CC BY) license (<https://creativecommons.org/licenses/by/4.0/>).

1. Introduction

The primary contributors to nickel production, ranking as the top six nations, include Indonesia, Russia, the Philippines, New Caledonia, Canada, and Australia. Consequently, Australia's mining sector, particularly in Western Australia, is relevant, accounting for approximately 6% of the global nickel market [1]. According to data provided by [2], Western Australia holds 96% of Australia's economic demonstrated resources (EDR), encompassing both nickel sulfide and lateritic nickel deposits, thereby solidifying its position as the foremost repository of nickel resources. Western Australia falls within the Archean Yilgarn Craton known to host nickel–copper–platinum group element (Ni-Cu-PGE) sulfide deposits in the volcanic-hosted komatiite magmas and lateritic nickel deposits. The craton also consists of greenstone belts like the Agnew–Wiluna Greenstone Belt, which

hosts Mt Keith, Perseverance, Yakabindie, and Honeymoon Well. Perseverance, along with Rocky's Reward and Harmony, is situated within the Leinster deposits, all of which are hosted by the metamorphosed Agnew–Wiluna Greenstone Belt [3,4]. The subsequent positions are held by Queensland, at 4.5% of the global Ni market, and Tasmania, at 0.2%. Notably, Queensland's deposits are predominantly lateritic, while Tasmania's deposits consist mainly of sulfidic nickel [5].

The central role of nickel across diverse sectors brings to light the crucial importance of sustainable extraction techniques and continuous exploration within nickel supply chains. As part of the effort to address this challenge, the current focus on sustainable objectives has resulted in a stabilization of nickel demand, particularly as the shift towards renewable and clean energy gains momentum to promote environmental sustainability. Amid this evolving landscape of sustainable practices and increasing nickel demand, it is important to acknowledge the essential role of pentlandite, a significant mineral source of nickel [6]. Recognizing the significance of pentlandite's abundance and extraction methods becomes paramount in meeting the requirements of environmental conservation and facilitating the global transition to cleaner energy sources, particularly given the gradual depletion of high-grade and easily treatable ores. Consequently, the mineral-processing industry faces the challenge of exploring solutions to effectively treat finely grained low-grade nickel sulfide ores [7], nickeliferous laterite [8], and more recently, tailings [9]. As the available options become limited, the concept of anthropogenic mining is gaining traction as a promoted approach.

Given this, the present study evaluates the technical feasibility of recovering nickel sulfide and subsequently upgrading nickel from a mining operation in Western Australia. The operation in question employs froth flotation to achieve approximately 82% nickel recovery. Notwithstanding, the nickel grade of the final concentrate averages 10% and presents an opportunity for upgrade. Although there have been earlier investigations to understand the effect of silicate minerals on nickel recovery and selectivity [10], there is still limited knowledge and fundamental understanding of the mechanisms involved in the beneficiation of pentlandite (NiFe sulfides) by flotation. In this paper, the outcome of detailed chemical and mineralogical characterization studies of a nickel sulfide concentrate is presented. The chemical composition of the sample was analyzed using inductively coupled plasma (ICP) optical emission spectrometry. Furthermore, size analysis using test sieves was carried out, after which the individual size fractions were analyzed via ICP-OES. The mineralogical composition, liberation characteristics, and mineral associations with key references to base metal sulfides were obtained using QEMSCAN analysis. Ultimately, the results obtained were used to discuss possible beneficiation techniques (gravity separation, magnetic separation, and froth flotation) that may be exploited to recover and subsequently enrich the nickel grade.

2. Materials and Methods

2.1. Raw Material

The nickel sulfide final concentrate was sourced from an existing nickel operation mine (Eastern Goldfields Region of Western Australia). The sample was collected from a flotation process comprising flash flotation and staged coarse and fine rougher flotations, each followed by two cleaner flotation stages. The primary reagents employed during the flotation process included guar gum as a gangue minerals depressant, sodium ethyl xanthate as a collector for nickel sulfide minerals, copper sulphate as a nickel sulfide activator, and polyfroth W55 as a frother. A block flowsheet of the process route is shown in Figure 1.

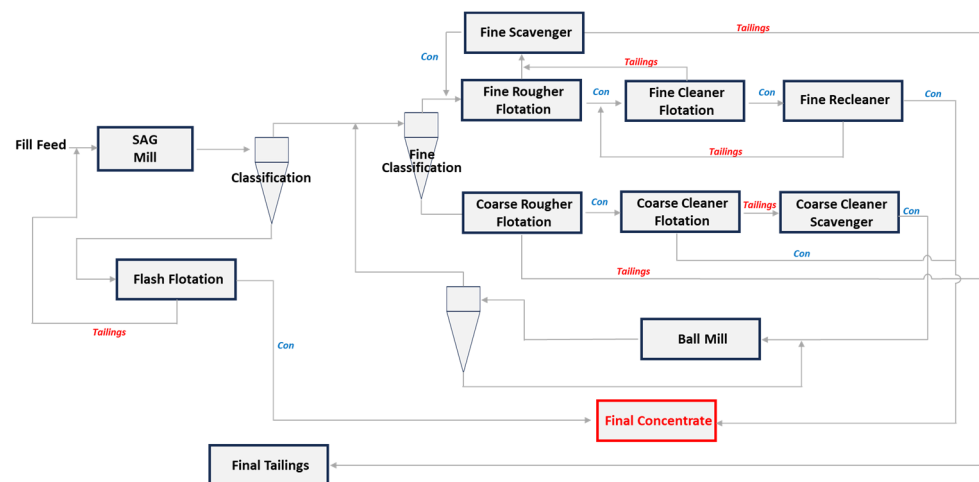


Figure 1. Flowsheet for the nickel operation.

2.2. Sample Preparation

A representative sample of 1 kg was obtained from the bulk material and dried at a temperature of 45 °C in the oven. Using a micro-standard riffle splitter (Laval Lab, Laval, QC, Canada), the material was split until the two separate subsamples each weighed about 100 g. The sub-samples underwent wet screening using the following sieves: 300, 212, 150, 106, 75, 53, 38, and 20 µm. The material retained on the respective screens were subsequently mounted in epoxy resin to produce blocks of 30 mm cross-sectional diameter, polished, and then carbon coated. The carbon coating provides a conductive layer that helps dissipate charges, leading to clearer images and more accurate data. The sample blocks were submitted for QEMSCAN analysis. The two undersize products from the 20 µm sieve were combined during the block formation. The other 100 g were riffle split for mineralogical and particle size distribution analyses, respectively.

2.3. Laser Diffraction Measurement

A Malvern Mastersizer 2000 (Malvern Instruments Ltd., Malvern, Worcestershire, UK) was used to ascertain the grain size distribution of the sample generated through laser diffraction. During the sample preparation stage, a subsample of the material was used to achieve a pulp concentration of approximately 30 wt.% in the presence of demineralized water and at room temperature. The suspension was agitated at a rate of 690 rpm for 10 min to ensure the complete dispersion of the mineral particles. All samples were measured in triplicate, and the combined data from these 15 measurements were used to establish the average particle size distribution.

2.4. ICP-OES Analysis

Inductively coupled plasma optical emission spectrometry was performed to determine the chemical composition of the concentrate. This process incorporated the utilization of lithium metaborate to digest the sample at a high temperature in a platinum (Pt) crucible to reduce any form of cross-contamination. Following this, the fused glass was subjected to digestion using nitric acid to ensure the complete dissolution of the ore before proceeding with the analysis. During the dissolution process, volatile elements, including silicates, were lost at high fusion temperatures. To incorporate quality control, the procedures included performing duplicates and the addition of blanks and reference materials into a rack of samples to measure the level of accuracy of the data.

2.5. Quantitative X-ray Diffraction (QXRD) Analysis

Quantitative X-ray diffraction was conducted to quantify the crystalline phases present in the nickel sulfide concentrates. The samples were measured twice, with the first sweep

focused on the full phase identification ranging from 2θ of 5 to 90 ($^{\circ}$), while the second analysis was focused on a narrower range of 43° to $53^{\circ}2\theta$. The scanning speed for both was 0.095° per second, with a step size of 0.039° . This approach was taken to investigate the distinct crystal structures of pyrrhotite. The X-ray powder diffractograms of the minerals were obtained using a PANalytical Empyrean diffractometer (Malvern Panalytical Ltd., Malvern, Worcestershire, UK) with radiation Cu-K α (40 kV and 40 mA) equipped with a graphite monochromator ($\lambda = 1.54056 \text{ \AA}$). Rietveld quantitative analysis was performed on the identified patterns using Xpert Highscore Plus and the associated reference database.

2.6. QEMSCAN Analysis

Automated mineralogical composition and particle characterization studies were carried out on the sample and quantitatively measured by QEMSCAN. The analysis made it possible to calculate the ratio of the elements of interest within each phase. QEMSCAN analysis also provided digital imaging capabilities by fully automating the acquisition of quantitative chemical and mineralogical data from a range of samples. The mineralogical data were expressed as the percentage volume of the sample and the cumulative volume of the different minerals in the sample forms of the mineralogical composition. Depending on the mineral physical characteristics, such as size, density, or flotation potential, in comparison to the gangue mineral mix, specific host minerals were singled out for in-depth analysis. Additionally, it was feasible to explore the textural connections between host minerals and the gangue minerals. The QEMSCAN utilized a two-dimensional mapping analysis to quantify the percentage mineral mass abundance, liberation, and locking characteristics of a standard group of particles referred to as the particle mineral analysis [11,12]. These techniques for characterization have been recognized as both effective and efficient for assessing nickel mineralization across various types of ores.

3. Results

3.1. Size Analysis

The particle size distribution (PSD) of the nickel concentrate, obtained through both hand sieving and Mastersizer analysis, is detailed in Table 1 and visually represented in Figure 2. According to the laser scattering data, the particle size distribution of the sample ranged from 0.1 to 1000 μm , with a P_{80} of 72 μm , whereas hand sieving yielded a P_{80} of 75 μm . Additionally, the manual sieving data showed that a higher proportion of the sample was found in the particle size fraction below the 38 μm sieve, constituting approximately half of the total sample mass. The data showed that the 150 μm sieve, which was considered the coarsest sieve, retained a total mass of 5.3% of the feed. This was followed by the 75 μm sieve, with about 94.79% of the sample particles passing through the sieve and with about 16.1% particles being retained. In a similar way, the 38 and 20 μm sieves retained oversized sample particles of about 28.8% and 15.3%, respectively. The total fine fraction was calculated from the 38 μm sieve using the sample block preparation as a guide, giving a total of 49.8 wt.%. Overall, the results indicated that the concentrate was generally with the bulk of the particles below 75 μm .

Table 1. Sieve analysis for particle size distribution.

Sieve Size (μm)	Weight Retained (g)	Percentage Retained (%)	Cumulative Retained (%)	Cumulative Passing (%)
−300 + 150	11.8	5.3	5.3	100.0
−150 + 75	36.0	16.2	21.5	94.7
−75 + 38	64.0	28.8	50.2	78.5
−38 + 20	34.0	15.3	65.5	49.8
−20	76.8	34.5	100	34.5
Total	223	100		

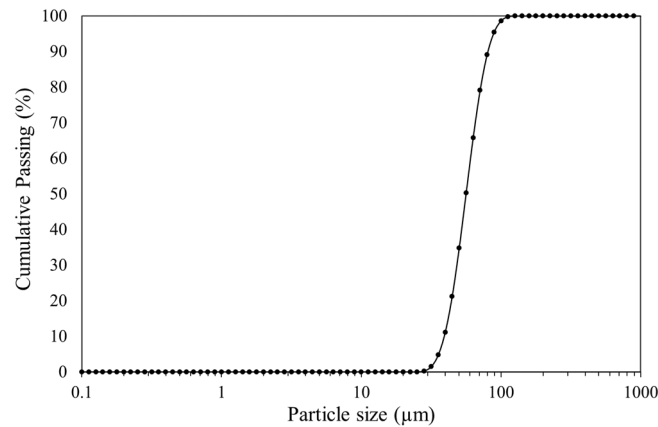


Figure 2. Particle size distribution of the nickel sulfide concentrate (P_{80} of 72 μm).

3.2. Chemical Composition

Bulk Elemental Composition

Table 2 illustrates the detailed chemical composition of the nickel sulfide sample, as determined by ICP-OES analysis. The results showed Ni contents ranging from 11.1% to 14.1%, with the highest concentration observed in the $-150 +75 \mu\text{m}$ size fraction. Also, Fe content demonstrated consistency across the various size fractions, with values ranging from 44% to 37%, with the lowest Fe grade (37%) reporting the $-20 \mu\text{m}$ size fraction. This was followed by a sulfur (S) content of about 31.2%, indicating the presence of sulfide minerals like pyrrhotite, violarite, and pyrite across all size fractions. Silicon (Si) content, on the other hand, increased from 1.3% to 5.2% as the particle size decreased. Aluminum (Al) and cobalt (Co) also exhibited consistent values across all particle size fractions. On the other hand, Cu content decreased from 1% to 0.6% with decreasing particle size, while Mg content increased as particle size decreased. A detailed distribution of the elements/metals across particle size ranges is shown in Figure 3.

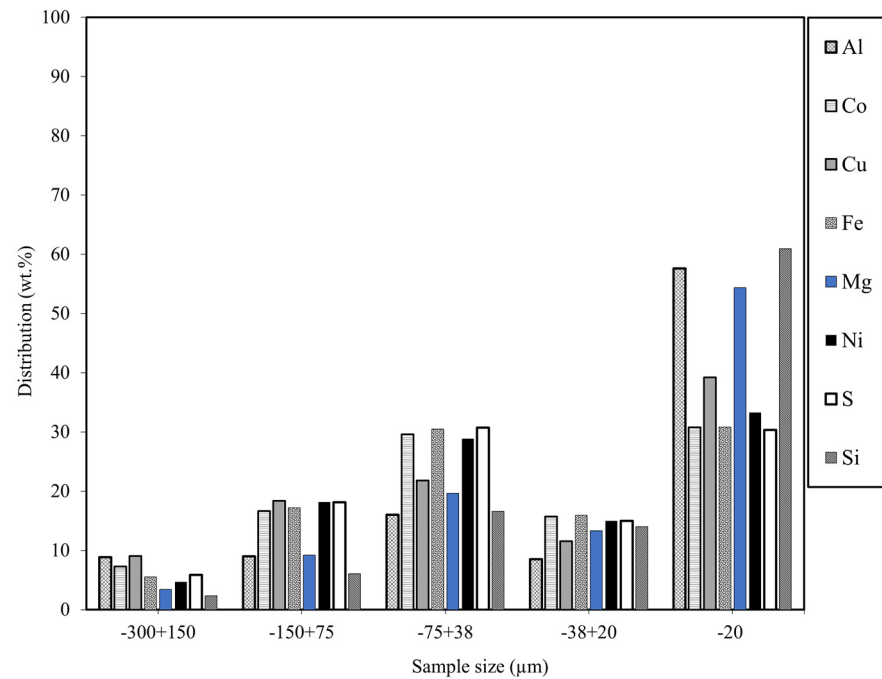


Figure 3. Elemental distribution of assays across particle size ranges.

Table 2. Elemental composition of concentrates used in the study.

Particle Size (μm)	Assays, %							
	Al	Co	Cu	Fe	Mg	Ni	S	Si
−300 + 150	0.3	0.4	1.0	43.2	1.7	11.1	34.4	1.3
−150 + 75	0.1	0.3	0.6	44.0	1.5	14.1	34.9	1.1
−75 + 38	0.1	0.3	0.4	43.9	1.8	12.6	33.3	1.7
−38 + 20	0.1	0.3	0.4	43.2	2.3	12.3	30.6	2.7
−20	0.3	0.3	0.6	37.0	4.2	12.1	27.4	5.2
Head (Calc.)	0.2	0.3	0.5	41.4	2.6	12.5	31.2	2.9

3.3. Mineralogical Composition

3.3.1. QXRD Analysis

The mineralogical composition of the sample as determined by X-ray diffraction is summarized in Table 3. According to the QXRD data, the concentrate sample was predominantly composed of pyrrhotite and pentlandite in almost equal amounts, with talc and magnetite as the major gangue minerals and trace amounts of albite, anorthite, brucite, clinocllore, and tochilinite. The notably high concentration of pyrrhotite suggests it is the main diluent of the grade of the concentrate. This observation is consistent with the results obtained from the ICP-OES analysis, further affirming the high iron content of about 43%. The identification of talc, a magnesium silicate mineral, aligns with the characterization of major gangue components in such ore formations [13]. Similarly, the detection of serpentine and magnesite further underscores the prevalence of magnesium-bearing minerals, contributing to the gangue composition of the concentrate. Reducing the pyrrhotite content through further beneficiation could lead to an increase in the nickel grade in the concentrate, with an associated increased market value. Given the information provided by the QXRD analysis, it is theorized that high pyrrhotite in the concentrate could be attributed to either pentlandite–pyrrhotite composite particles or to the presence of fine liberated pyrrhotite particles carried over to the concentrate by entrainment in the flotation process. Additional grinding might be necessary for the former to fully liberate pentlandite–pyrrhotite composite particles in the sample. However, it is imperative to acknowledge that such measures may concurrently heighten pyrrhotite entrainment during flotation. This is discussed with the QEMSCAN analysis further below.

Table 3. Mineralogical compositions of concentrates used in the study.

Mineral Phase	Content (wt.%)
Pentlandite	40
Pyrrhotite	44
Talc	6
Magnetite	5
Violarite	2
Serpentine	2
Magnesite	1
Pyrite	<1
Olivine	<1
Quartz	<1
Total	100

Concurrently, an investigation into the different crystal structures of pyrrhotite was conducted using the QXRD to elucidate which form of pyrrhotite polymorph (monoclinic and or hexagonal) was present. The results from the crystallographic studies revealed that the pyrrhotite contained both monoclinic and hexagonal crystal patterns. Figure 4

shows the identified monoclinic and hexagonal pyrrhotite peaks, which are consistent with crystallographic studies conducted, although some variations may occur [14–18].

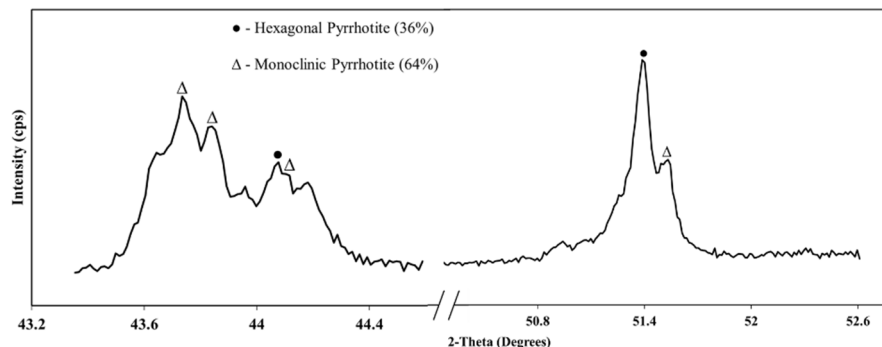


Figure 4. QXRD (Cu K α) diffractograms for the monoclinic and hexagonal pyrrhotite with two coordinates relative intensities (2 θ).

3.3.2. Distribution of Nickel and Gangue Minerals

QEMSCAN analysis was carried out to quantify the mineral masses present by assigning pixels with specific mineral identities. Pentlandite particles and nickel-bearing minerals, such as pyrrhotite, were identified. Different proportions of pyrite, talc, olivine, carbonates, serpentine, violarite, chalcopyrite, gersdorffite, chromite, quartz, millerite, and ilmenite were also identified. Figure 5 shows that the highest pyrrhotite content, averaging 52%, was in the finer size fraction (<38 μm). The average pyrite content in the concentrate increased from 6% to 14% with an increasing size fraction. The sample comprised 30% pentlandite in the $-300 + 150 \mu\text{m}$, 30% in the $-150 + 75 \mu\text{m}$, 31% in $-75 + 38 \mu\text{m}$, and 28% in the $-38 + 20 \mu\text{m}$ blocks, with a minor amount of violarite (less than 2%). Furthermore, 3%, 2%, 1%, and 1% of chalcopyrite grains were found in the $-300 + 150 \mu\text{m}$, $-150 + 75 \mu\text{m}$, $-75 + 38 \mu\text{m}$, and $-38 + 20 \mu\text{m}$ blocks, respectively. In the $-38 + 20 \mu\text{m}$ size fraction, talc (cummingtonite) had the highest abundance of 6%, with other silicates contributing 2.7%. Also, the compositions of oxides in the respective size fractions (high to low) were 2.6%, 1.8%, 1.4%, and 1.5%, which averaged a 32% liberation. Overall, pyrrhotite was the most abundant mineral in the concentrate, constituting 52% of the $-38 + 20 \mu\text{m}$ size fraction, compared to the targeted mineral, pentlandite, which made up 28% of the concentrate. This suggests the need to employ beneficiation strategies to potentially remove the entrained pyrrhotite.

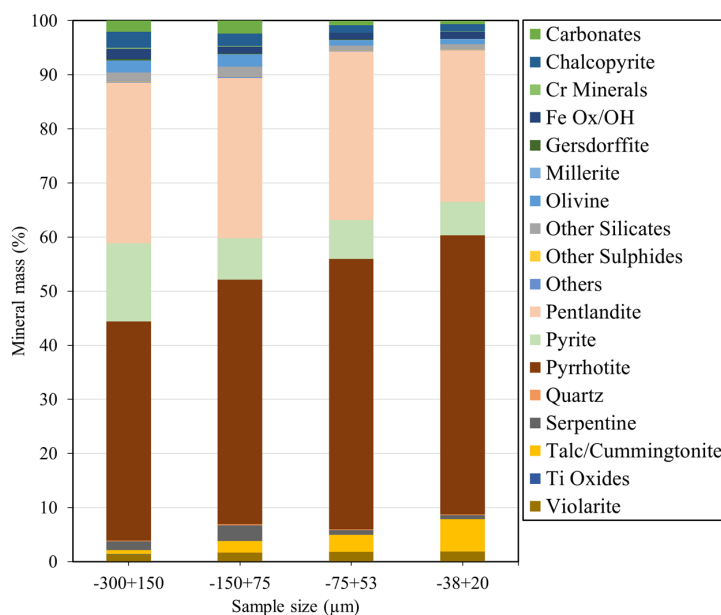


Figure 5. Mineral distribution of nickel and associated gangue minerals.

3.3.3. Mineral Liberation and Locking Characteristics

Figure 6 shows the mineral liberation with respect to the various particle size fractions and the locking ratio or locking category data. Mineral locking ratio or category of the particular mineral was calculated using the total area percent of the minerals, particle size, and the associated mineral of interest [19]. The minerals were categorized based on their area percent of surface exposure (x): liberated ($x \geq 90\%$), high middling ($60 \leq x < 90\%$), low middling ($30 \leq x < 60\%$), and locked ($x < 30\%$). It is observed from Table 4 that 91% of nickel iron (NiFe) sulfides in the $-38 + 20 \mu\text{m}$ fraction were liberated, followed by the $-75 + 38 \mu\text{m}$, with a high middling percentage of 88%. NiFe sulfides within the $-300 + 150 \mu\text{m}$ and $-150 + 75 \mu\text{m}$ fractions had slightly lower compositions of liberated particles of 70% and 78%, respectively. From Table 4, the liberation data indicated almost a complete liberation of NiFe sulfides, silicates, and Fe sulfides in the $-38 + 20 \mu\text{m}$ particle size fraction, revealing their potential impacts on the selectivity and grade of the concentrate. The chalcopyrite and oxides, on the other hand, were locked throughout the size fractions and would likely form part of the composite binary, ternary, and composite particles. Overall, the locking ratios support the mineral mass liberation data, where it was observed that the NiFe sulfides were liberated in the $-38 + 20 \mu\text{m}$ size fraction, with 7 wt.% pentlandite binary-locked with Fe sulfides.

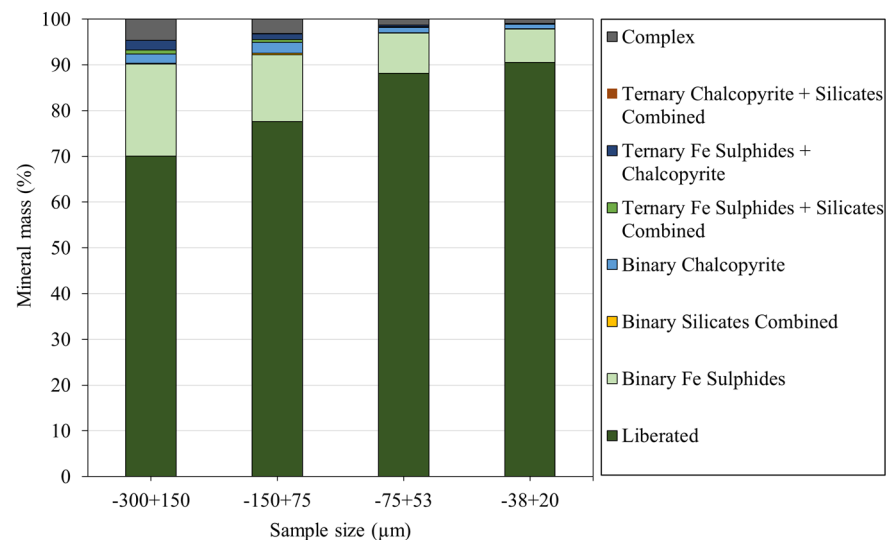


Figure 6. NiFe sulfide mineral locking profiles at different size fractions: binary, ternary, and complex mineral associations.

Table 4. Summary of the detailed mineral liberations and their associations.

Sample	$-300 + 150 \mu\text{m}$	$-150 + 75 \mu\text{m}$	$-75 + 38 \mu\text{m}$	$-38 + 20 \mu\text{m}$
NiFe Sulfides	70	78	88	91
Fe Sulfides	69	81	89	92
Chalcopyrite	36	50	59	72
Silicates Combined	50	70	85	92
Oxides	21	22	35	49

The liberation analysis revealed significant trends across particle size fractions. About 70% of the NiFe sulfides were liberated in the coarsest ($-300 + 150 \mu\text{m}$) fraction, whereas in the finest fraction ($-38 + 20 \mu\text{m}$), about 91% of NiFe sulfides were liberated. Furthermore, predominant Fe sulfides in the finest fraction (92%) suggests the possibility of pyrrhotite and pyrite reporting into the concentrate via entrainment or poor selectivity of the downstream flotation stages. Figure 7 illustrates the distributions of both pentlandite (NiFe sulfides) and

pyrrhotite (Fe sulfides) across different size ranges and their liberation categories. It can be seen from Figure 7 that both pentlandite and pyrrhotite were liberated across the particle size ranges, and hence, further grinding will not be required. However, this suggests that beneficiation strategies will have to be incorporated to avoid mainly pyrrhotite and other Fe sulfides from reporting into the concentrate. Also, the silicates in the fine fraction followed a similar trend to the NiFe sulfides and Fe sulfides. The liberation percentages for the silicates consistently increased with decreasing particle size from 50% in the $-300 + 150 \mu\text{m}$ fraction to 92% in the $-38 + 20 \mu\text{m}$ fraction. The oxides, which are magnetite and hematite, show a notable increase in the $-38 + 20 \mu\text{m}$ fraction. Typically, the occurrence of these minerals in the finer particle size of the concentrate could potentially affect the enrichment ratio of nickel.

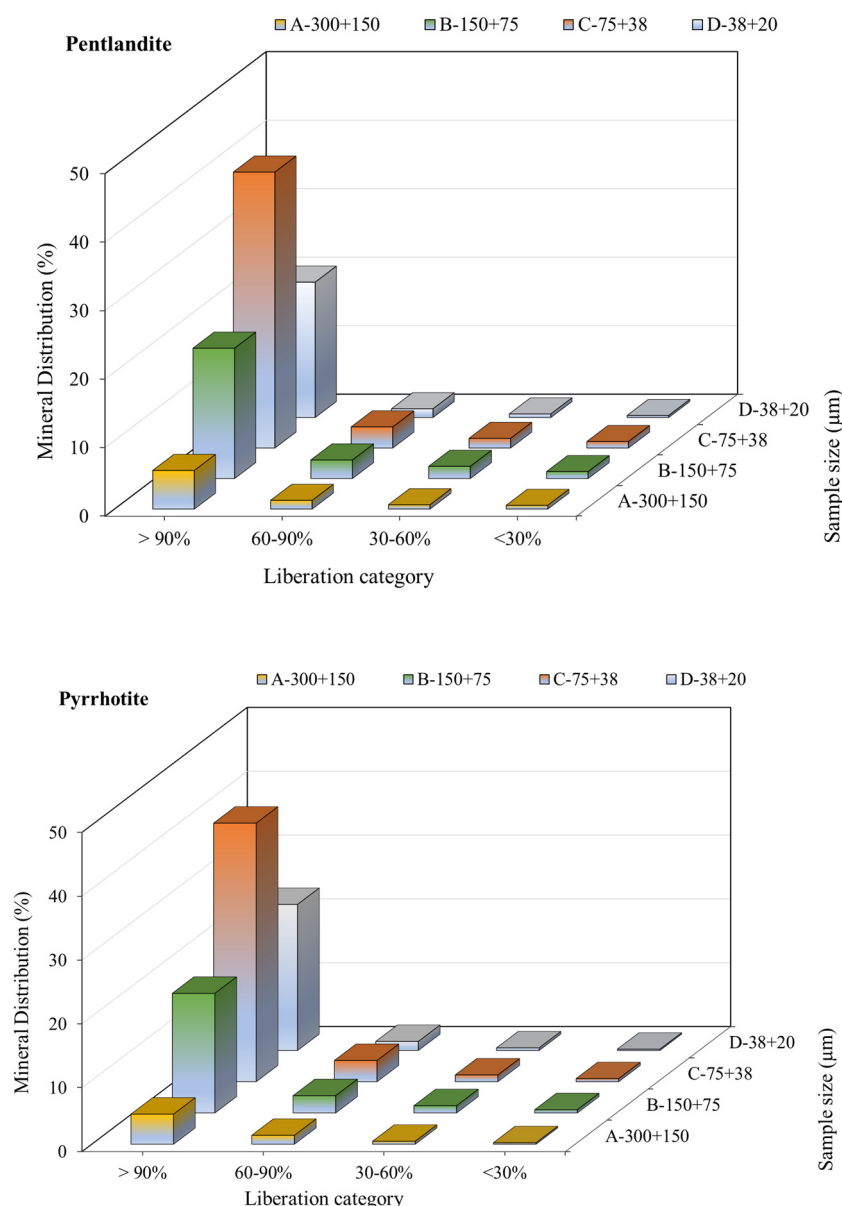
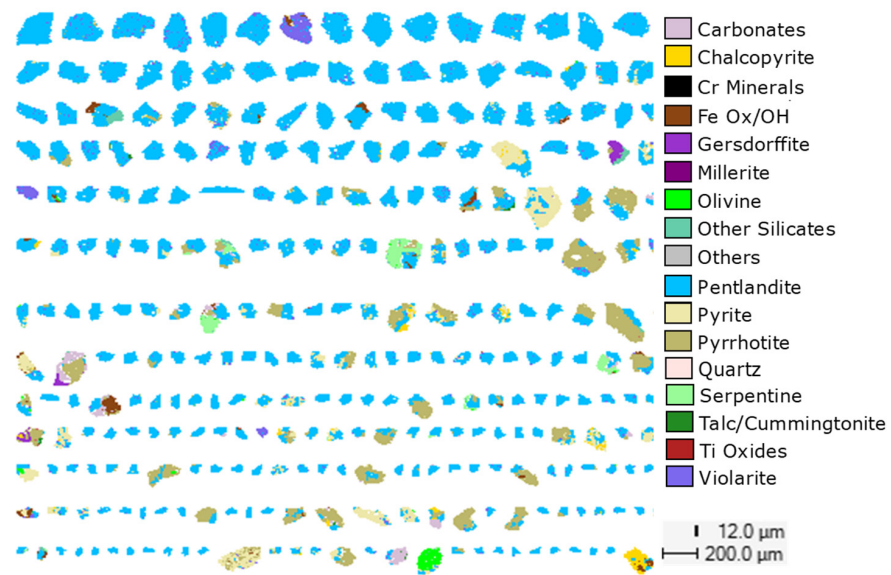
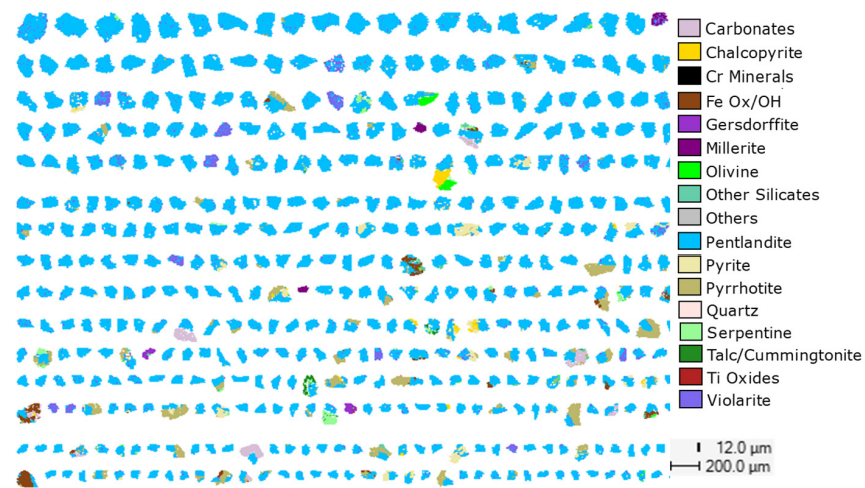


Figure 7. Particle size and liberation category of pentlandite and pyrrhotite minerals.

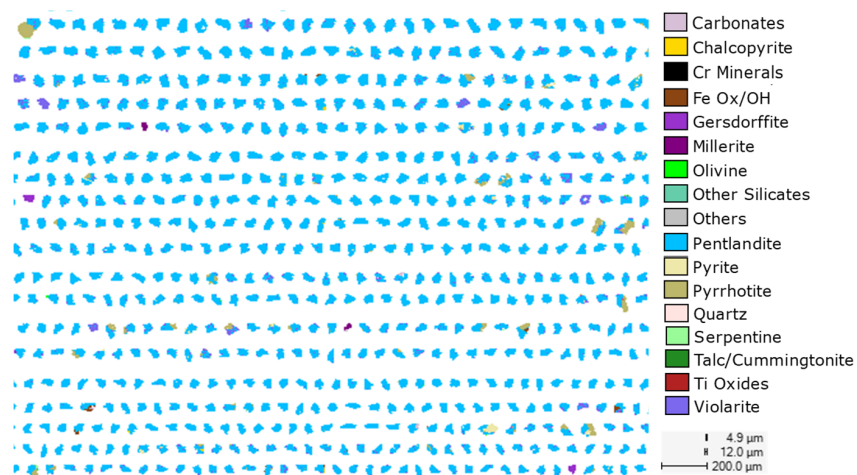
In addition to the locking analysis, QEMSCAN mineral maps showing the association and liberation of mineral phases within the $-300 + 150$, $-150 + 75$, $-75 + 38$, and $-38 + 20 \mu\text{m}$ size fractions are presented in Figure 8a–d. The particle view showed that the concentrate was dominated by a mixture of NiFe sulfides and mostly Fe Sulfides, with varying particle size distributions.



(a)



(b)



(c)

Figure 8. Cont.

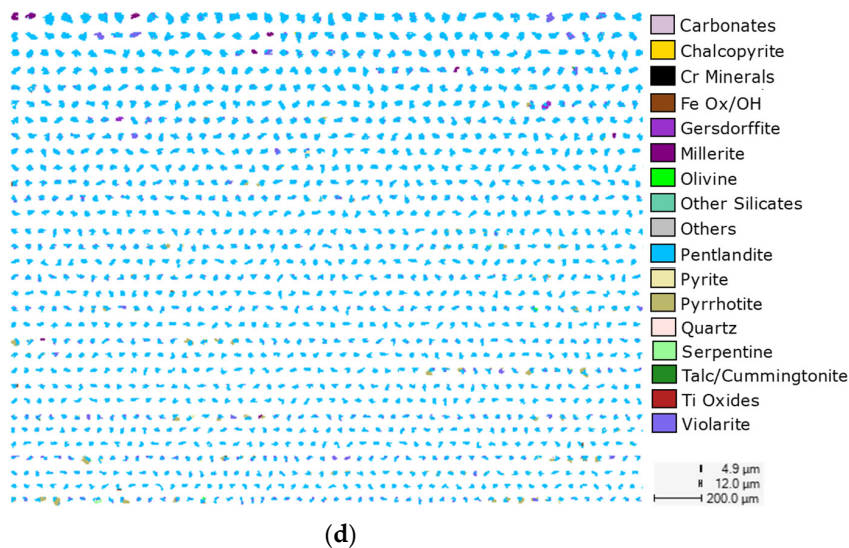


Figure 8. (a) QEMSCAN mineral map of the $-300 + 150 \mu\text{m}$ size fraction. (b) QEMSCAN mineral map of the $-150 + 75 \mu\text{m}$ size fraction. (c) QEMSCAN mineral map of the $-75 + 38 \mu\text{m}$ size fraction. (d) QEMSCAN mineral map of the $-38 + 20 \mu\text{m}$ size fraction.

4. QEMSCAN Data Validation

Quality assurance and quality control (QA/QC) checks are essential for ensuring the consistency and accuracy of the mineralogical data generated [20]. The study employed a comprehensive validation strategy by comparing the QEMSCAN assay with those derived from a chemical assay obtained via ICP-OES analysis. To visually represent the relationship between the two analytical methods, a parity plot of the assays of major elements obtained using the QEMSCAN was compared with that obtained from the ICP-OES, as shown in Figure 9. The broken line in Figure 9 follows a 1:1 relationship, where the equation is $y = x$. The correlation coefficient value of the two variables was higher than 0.9. The plotted data points on the graph illustrated a positive correlation between the chemical assays and QEMSCAN assays for various elements within the samples under investigation. The positive correlation observed in the graphical representation suggests that variations in the mineralogical composition, as identified by QEMSCAN, agrees with that by ICP-OES. Although there are some discrepancies, further checks showed that the observed variations in S and Ni fall within the acceptable limits and could possibly be attributed to misestimation by QEMSCAN during the respective analyses.

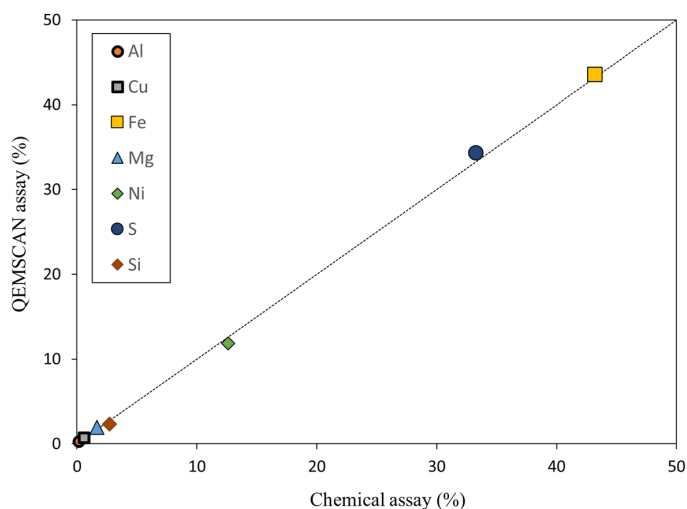


Figure 9. Graphical comparison of ICP-OES analyses with QEMSCAN-derived element concentrations.

5. Possible Beneficiation Approaches

Typically, the processing of most ores involves initial comminution for mineral liberation, followed by sizing for classification. Subsequently, preconcentration methods, such as froth flotation, magnetic separation, and gravity separation, are applied to separate various mineral–gangue associations. In the case of nickel sulfide ore beneficiation, the primary methods are flotation [21] and magnetic separation [22], with gravity separation [23] often utilized as an additional approach. Drawing insights from QEMSCAN data, the beneficiation approaches will be explored and discussed.

5.1. Gravity Separation

Gravity separation is a mineral-processing technique that capitalizes on the differences in density between minerals for separation [24]. For efficient separation using this technique, there ought to be a distinct difference between the targeted mineral and the unwanted mineral [25]. Considering the specific gravities of pentlandite (4.6 to 5.0 g/cm³) [26] and pyrrhotite (4.5 to 4.7 g/cm³) [27], it becomes evident that their densities are quite similar, posing challenges for effective separation using this method. To that effect, alternative techniques, such as flotation or magnetic separation, are typically employed for separating pentlandite and pyrrhotite, due to their comparable densities.

5.2. Magnetic Separation

Magnetic separation is a physical separation technique that segregates highly magnetic (ferromagnetic) minerals from the less magnetic (paramagnetic) and non-magnetic (diamagnetic) minerals using the application of different magnetic field intensities. Ferromagnetic and paramagnetic minerals exhibit attraction along the lines of an applied magnetic field, whereas a diamagnetic mineral particle experiences repulsion from the magnetic field lines [28–30]. Pyrrhotite is a sulfide mineral known to occur in both magnetic (monoclinic) and non-magnetic (hexagonal) forms [31]. According to a study conducted by [3,32], the Leinster region is associated with variable proportions of ferromagnetic monoclinic pyrrhotite to antiferromagnetic hexagonal pyrrhotite. The QXRD report confirmed that 64% of the entire pyrrhotite is in the monoclinic form, with the remaining portion being composed of hexagonal pyrrhotite. Considering this, it would be efficient to subject the sample to magnetic separation to eliminate all forms of monoclinic pyrrhotite contents in the processing route. In the beneficiation of pentlandite [33–35], magnetic separation was employed to produce nickel-rich concentrate while rejecting a significant proportion of pyrrhotite. While magnetic separation has historically been utilized for ores of this nature, the finer particles within the sample could potentially render magnetic separation less effective, due to the insufficient strength of the magnetic force [36].

5.3. Froth Flotation

Flotation is a mineral-processing technique that involves the selective separation of targeted minerals from gangue minerals by capitalizing on the differences in their surface properties [24]. In Ref. [37], the impact of mineral surface properties in relation to wetting films was discussed. The overall wetting behavior of mineral surfaces was found to strongly depend on the surface properties. As such, different mineral surfaces have different responses to bubble attachment. Mineral surfaces that are easily wetted by liquids and have a low affinity for bubble attachment are termed as hydrophilic. Surfaces that are easily attached to air bubbles allow them to rise to the surface of a flotation cell and form a froth [29,38–40].

It was evident from the detailed characterization studies that the concentrate contained high amounts of pyrrhotite (52 wt.%) at the finest size fraction, with smaller quantities of other sulfide minerals (6 wt.%) and silicate minerals (9 wt.%) present. Complete separation between pyrrhotite and pentlandite has posed a persistent challenge over the years. This difficulty arises from the prevalence of iron sulfides in complex sulfide ores, compounded by their nickeliferous nature [41]. However, more recent studies by [33], as well as [34],

indicate a potential breakthrough in achieving effective separation despite these challenges. Also, from the studies conducted by [33], it was observed that upon the introduction of 1.5 kg/t sodium metabisulphite (SMBS) and 0.35 kg/t triethylenetetramine (TETA), Ni grade increased from 3% to about 24% in a flotation study. This upgrade clearly surpassed the theoretical maximum Ni grade in the feed.

Elsewhere, ref. [34] proposed a dual approach involving chelating agents and electrochemical alterations to suppress pyrrhotite recovery. Specifically, while controlling pulp potential at $-50 < Eh < +50$ mV, it was observed that the highest pyrrhotite depression (2.5%) occurred at $Eh = 50$ mV, with the highest pentlandite recovery (98.2%) obtained at -25 mV. Furthermore, the use of chelating agents in this process included diethylenetriamine (DETA) at a concentration of 225 g/t and sulfite at 450 g/t. The results from these investigations suggested that chelating agents and redox potential are key pointers in achieving selective nickel flotation recovery.

Improved liberation of pyrrhotite and pentlandite minerals at a fine size fraction and the possible entrainment of gangue pyrrhotite are considered in the froth flotation. In most flotation circuits, the mass pull of the circuit is significantly increased to improve the recovery of pentlandite. This comes at a grade deficit depicted in classical grade-recovery plots [42]. Moreso, fine particle flotation is characterized by froth instability, high reagents consumption, and the possibilities of achieving low concentrate grades and recoveries [43].

Recognizing these complexities, various methods, such as the introduction of ultrafine bubbles, two-stage reactor separator flotation cells, and particle agglomeration/floc flotation methods, have been considered to address these challenges [44–46]. Given the presence of high pyrrhotite in the finest fraction, the utilization of two-stage reactor separator cells, such as the Reflux flotation cell (RFC), Jameson cell, and Imhoflot cell, could be beneficial in solving the challenges of pyrrhotite entrainment. More specifically, the RFC, a novel flotation cell, demonstrated successful applications in floating fine-grained minerals such as copper, coal, iron, and nickel ores [47–49]. The RFC features a downcomer that promotes high collision efficiency through frequent particle–bubble collisions [50]. It also includes a reversed fluidized bed and inclined channels, which utilize a Boycott effect to segregate bubbles from the tailings stream [51,52]. The cell also incorporates a wash water system to create a bubbly zone, preventing hydrophilic gangue minerals from being collected into the concentrate. Based on data presented by [48,53,54], future efforts could be directed towards developing a methodology focused on reducing pyrrhotite entrainment using the RFC.

6. Conclusions

The mineralogical characterization and possible beneficiation strategies of a nickel sulfide concentrate from a Western Australian deposit were investigated to improve the nickel grade. Mineralogical studies indicated that the ore contains about 30 wt.% pentlandite and 70 wt.% gangue minerals. The nickel sulfide content is distributed at all size fractions; however, iron sulfides are more pronounced in the finer fraction (<20 μm). QEMSCAN studies alongside QXRD revealed that pentlandite, pyrrhotite, talc, magnetite, violarite, serpentine, magnesite, pyrite, olivine, and quartz minerals were present in the sample. The characterization results of the concentrate also indicated that there is a potential of Fe sulfides and silicates combined being entrained, due to the high percentages recorded in the finer fractions.

It is projected that the concentrate can be further enriched by the removal of pyrrhotite (monoclinic), magnetite, and magnesite through magnetic separation. Froth flotation can be utilized for rejecting hexagonal pyrrhotite, chalcopyrite, and all forms of Fe sulfides present in the ore. A specific challenge arises from very fine pyrrhotite particles disseminated within the concentrate. It is also proposed that fine pyrrhotite entrained in the pulp stream during froth collection may have contributed to the high pyrrhotite content in the concentrate. However, novel flotation cells/technologies with the outlined beneficiation strategies hold promise for advancing fine/ultrafine nickel mineral upgrade and recovery with reduced gangue minerals entrainment.

Author Contributions: L.D.A.: conceptualization, visualization, formal analysis, investigation, methodology, and writing—original draft. M.Z.: conceptualization, supervision, and writing—review and editing. W.S.: conceptualization, writing—review and editing, supervision, funding acquisition, and project administration. G.B.A.-W.: conceptualization, supervision, investigation, writing—review and editing, and project administration. All authors have read and agreed to the published version of the manuscript.

Funding: This research was funded by the Australian Research Council for the ARC Centre of Excellence for Enabling Eco-Efficient Beneficiation of Minerals, grant number CE200100009.

Data Availability Statement: Data will be made available on request.

Acknowledgments: The authors also acknowledge the facilities and technical assistance of the staff of Microscopy Australia at the Future Industries Institute, University of South Australia. This work used the NCRIS and Government of South Australia-enabled Australian National Fabrication Facility—South Australian Node (ANFF-SA).

Conflicts of Interest: The authors declare that they have no known competing financial interests or personal relationships that could have appeared to influence the work reported in this paper.

References

1. Michele, M. *US Geological Survey, Mineral Commodity Summaries*; January 2022; National Minerals Information Center: Reston, VA, USA, 2022.
2. Dulfer, H.; Milligan, P.R.; Coghlan, R.; Czarnota, K.; Highet, L.M.; Champion, D.C.; Skirrow, R.G. *Potential for Intrusion-Hosted Ni-Cu-PGE Sulfide Deposits in Australia: A Continental-Scale Analysis of Mineral System Prospectivity*; Geoscience Australia: Canberra, Australia, 2016.
3. Williams, N.C. Mass and magnetic properties for 3D geological and geophysical modelling of the southern Agnew–Wiluna Greenstone Belt and Leinster nickel deposits, Western Australia. *Aust. J. Earth Sci.* **2009**, *56*, 1111–1142. [[CrossRef](#)]
4. Cahill, J.; Lee, M. Ground control at Leinster nickel operations. *J. S. Afr. Inst. Min. Metall.* **2006**, *106*, 471–478.
5. Teh, M.; Pheeney, J. *Australian Resource Reviews: Nickel 2020*; Geoscience Australia: Canberra, Australia, 2021.
6. Legrand, D.L.; Bancroft, G.M.; Nesbitt, H.W. Surface characterization of pentlandite, (Fe,Ni)₉S₈, by X-ray photoelectron spectroscopy. *Int. J. Miner. Process.* **1997**, *51*, 217–228. [[CrossRef](#)]
7. Senior, G.; Thomas, S. Development and implementation of a new flowsheet for the flotation of a low grade nickel ore. *Int. J. Miner. Process.* **2005**, *78*, 49–61. [[CrossRef](#)]
8. Tian, H.; Pan, J.; Zhu, D.; Yang, C.; Guo, Z.; Xue, Y. Improved beneficiation of nickel and iron from a low-grade saprolite laterite by addition of limonitic laterite ore and CaCO₃. *J. Mater. Res. Technol.* **2020**, *9*, 2578–2589. [[CrossRef](#)]
9. Botelho Junior, A.B.; Dreisinger, D.B.; Espinosa, D.C.R. A Review of Nickel, Copper, and Cobalt Recovery by Chelating Ion Exchange Resins from Mining Processes and Mining Tailings. *Min. Metall. Explor.* **2019**, *36*, 199–213. [[CrossRef](#)]
10. Ayedzi, L.D.; Abaka-Wood, G.B.; Zanin, M.; Skinner, W. Electrokinetic study of pentlandite and quartz for froth flotation separation. In Proceedings of the 18th Procemin-Geomet 2022, Virtual, 5–7 October 2022; pp. 184–193.
11. Grammatikopoulos, T.; Mercer, W.; Gunning, C.; Prout, S. Quantitative characterization of the REE minerals by QEMSCAN from the Nechalacho Heavy Rare Earth Deposit, Thor Lake Project, NWT, Canada. *SGS Miner. Serv. Tech. Pap.* **2011**, *7*, 1–11.
12. Abaka-Wood, G.B.; Addai-Mensah, J.; Skinner, W. The Use of Mining Tailings as Analog of Rare Earth Elements Resources: Part 1—Characterization and Preliminary Separation. *Miner. Process. Extr. Metall. Rev.* **2022**, *43*, 701–715. [[CrossRef](#)]
13. Duuring, P.; Hassan, L.; Zelic, M.; Gessner, K. Geochemical and spectral footprint of metamorphosed and deformed VMS-style mineralization in the Quinns district, Yilgarn Craton, Western Australia. *Econ. Geol.* **2016**, *111*, 1411–1438. [[CrossRef](#)]
14. Khoso, S.A.; Gao, Z.; Tian, M.; Hu, Y.; Sun, W. Adsorption and depression mechanism of an environmentally friendly reagent in differential flotation of Cu–Fe sulphides. *J. Mater. Res. Technol.* **2019**, *8*, 5422–5431. [[CrossRef](#)]
15. Koulialias, D.; Kind, J.; Charilaou, M.; Weidler, P.; Löffler, J.; Gehring, A. Variable defect structures cause the magnetic low-temperature transition in natural monoclinic pyrrhotite. *Geophys. J. Int.* **2016**, *204*, 961–967. [[CrossRef](#)]
16. Qiu, T.; Zhang, C.; Yang, L.; Wang, J.; Zhao, G.; Yan, H.; Wu, H.; Qiu, X.; Yang, B.; Liao, R. Effect of Electrochemical Interaction between Chalcopyrite and Hexagonal Pyrrhotite on Flotation Separation. *Minerals* **2023**, *13*, 1303. [[CrossRef](#)]
17. Lu, P.; Chen, T.; Liu, H.; Li, P.; Peng, S.; Yang, Y. Green preparation of nanoporous pyrrhotite by thermal treatment of pyrite as an effective Hg (II) adsorbent: Performance and mechanism. *Minerals* **2019**, *9*, 74. [[CrossRef](#)]
18. Chareev, D.A.; Voronin, M.V.; Osadchii, E.G. Thermodynamic study of monoclinic pyrrhotite in equilibrium with pyrite in the Ag-Fe-S system by solid-state electrochemical cell technique. *Am. Mineral.* **2014**, *99*, 2031–2034. [[CrossRef](#)]
19. Fosu, S.; Pring, A.; Skinner, W.; Zanin, M. Characterisation of coarse composite sphalerite particles with respect to flotation. *Miner. Eng.* **2015**, *71*, 105–112. [[CrossRef](#)]
20. Edahbi, M.; Benzaazoua, M.; Plante, B.; Doire, S.; Kormos, L. Mineralogical characterization using QEMSCAN® and leaching potential study of REE within silicate ores: A case study of the Matamec project, Québec, Canada. *J. Geochem. Explor.* **2018**, *185*, 64–73. [[CrossRef](#)]

21. Kirjavainen, V.; Heiskanen, K. Some factors that affect beneficiation of sulphide nickel–copper ores. *Miner. Eng.* **2007**, *20*, 629–633. [[CrossRef](#)]
22. Lu, J.; Yuan, Z.; Li, M.; Zhao, X.; Tong, Z.; Li, L.; Qi, S. The role of sodium oleate (NaOL) in the magnetic separation of pentlandite from serpentine using magnetic coating. *Powder Technol.* **2019**, *345*, 492–500. [[CrossRef](#)]
23. Yüce, A.E.; Bulut, G.; Boylu, F.; Önal, G. Process Flowsheet Development for Beneficiation of Nickel Ore. *Miner. Process. Extr. Metall. Rev.* **2007**, *29*, 57–67. [[CrossRef](#)]
24. Wills, B.A.; Finch, J. Wills' mineral processing technology: An introduction to the practical aspects of ore treatment and mineral recovery. In *Technology & Engineering*; Butterworth-Heinemann: Oxford, UK, 2015; p. 512.
25. Abaka-Wood, G.B.; Quast, K.; Zanin, M.; Addai-Mensah, J.; Skinner, W. A study of the feasibility of upgrading rare earth elements minerals from iron-oxide-silicate rich tailings using Knelson concentrator and Wilfley shaking table. *Powder Technol.* **2019**, *344*, 897–913. [[CrossRef](#)]
26. Bulatovic, S. Flotation of Nickel and Nickel–Copper Ores. In *Handbook of Flotation Reagents*; Elsevier Science & Technology Books: Amsterdam, The Netherlands, 2007; pp. 401–441.
27. Ikotun, B.D.; Adams, F.V.; Ikotun, A.G. Application of three xanthates collectors on the recovery of nickel and pentlandite in a low-grade nickel sulfide ore using optimum flotation parameters. *Part. Sci. Technol.* **2017**, *35*, 462–471. [[CrossRef](#)]
28. Abaka-Wood, G.B.; Addai-Mensah, J.; Skinner, W. Magnetic separation of monazite from mixed minerals. In *Chemeca 2016: Chemical Engineering-Regeneration, Recovery and Reinvention*; Engineers Australia: Melbourne, VIC, Australia, 2016.
29. Abaka-Wood, G.; Addai-Mensah, J.; Skinner, W. Review of flotation and physical separation of rare earth element minerals. In Proceedings of the 4th UMaT Biennial International Mining and Mineral Conference, Tarkwa, Ghana, 3–6 August 2016.
30. Oberteuffer, J. Magnetic separation: A review of principles, devices, and applications. *IEEE Trans. Magn.* **1974**, *10*, 223–238. [[CrossRef](#)]
31. Becker, M.; Villiers, J.d.; Bradshaw, D. The flotation of magnetic and non-magnetic pyrrhotite from selected nickel ore deposits. *Miner. Eng.* **2010**, *23*, 1045–1052. [[CrossRef](#)]
32. Perring, C.S. A 3-D geological and structural synthesis of the Leinster area of the Agnew-Wiluna belt, Yilgarn craton, Western Australia, with special reference to the volcanological setting of komatiite-associated nickel sulfide deposits. *Econ. Geol.* **2015**, *110*, 469–503. [[CrossRef](#)]
33. Kelebek, S.; Tukul, C. Separation of nickeliferous hexagonal pyrrhotite from pentlandite in Ni-Cu sulphide ores: Recovery by size performance. *Miner. Eng.* **2018**, *125*, 223–230. [[CrossRef](#)]
34. Manouchehri, H.R. Pyrrhotite flotation and its selectivity against pentlandite in the beneficiation of nickeliferous ores: An electrochemistry perspective. *Min. Metall. Explor.* **2014**, *31*, 115–125. [[CrossRef](#)]
35. Zhou, X.; Feng, B. The effect of polyether on the separation of pentlandite and serpentine. *J. Mater. Res. Technol.* **2015**, *4*, 429–433. [[CrossRef](#)]
36. Arol, A.I.; Aydogan, A. Recovery enhancement of magnetite fines in magnetic separation. *Colloids Surf. A Physicochem. Eng. Asp.* **2004**, *232*, 151–154. [[CrossRef](#)]
37. Krasowska, M.; Malysa, K. Wetting films in attachment of the colliding bubble. *Adv. Colloid Interface Sci.* **2007**, *134–135*, 138–150. [[CrossRef](#)]
38. Abaka-Wood, G.B.; Addai-Mensah, J.; Skinner, W. A study of flotation characteristics of monazite, hematite, and quartz using anionic collectors. *Int. J. Miner. Process.* **2017**, *158*, 55–62. [[CrossRef](#)]
39. Ralston, J.; Fornasiero, D.; Mishchuk, N. The hydrophobic force in flotation—a critique. *Colloids Surf. A Physicochem. Eng. Asp.* **2001**, *192*, 39–51. [[CrossRef](#)]
40. van Oss, C.J. *The Water–Air Interface, in Interface Science and Technology*; Elsevier: Amsterdam, The Netherlands, 2008; pp. 149–160.
41. Kelebek, S.; Tukul, C. The effect of sodium metabisulfite and triethylenetetramine system on pentlandite–pyrrhotite separation. *Int. J. Miner. Process.* **1999**, *57*, 135–152. [[CrossRef](#)]
42. Wills, B.; Napier–Munn, T. *Mineral Processing Technology*; Elsevier Science & Technology Books: Amsterdam, The Netherlands, 2006; pp. 267–352.
43. Farrokhpay, S.; Filippov, L.; Fornasiero, D. Flotation of Fine Particles: A Review. *Miner. Process. Extr. Metall. Rev.* **2021**, *42*, 473–483. [[CrossRef](#)]
44. Jameson, G.J. New directions in flotation machine design. *Miner. Eng.* **2010**, *23*, 835–841. [[CrossRef](#)]
45. Hassanzadeh, A.; Safari, M.; Hoang, D.H.; Khoshdast, H.; Albijanic, B.; Kowalczyk, P.B. Technological assessments on recent developments in fine and coarse particle flotation systems. *Miner. Eng.* **2022**, *180*, 107509. [[CrossRef](#)]
46. Li, C.; Zhang, H. Surface nanobubbles and their roles in flotation of fine particles—A review. *J. Ind. Eng. Chem.* **2022**, *106*, 37–51. [[CrossRef](#)]
47. Leonida, C. Floating New Ideas. *Eng. Min. J.* **2022**, *223*, 40–45.
48. Jiang, K.; Dickinson, J.E.; Galvin, K.P. The kinetics of Fast Flotation using the Reflux Flotation Cell. *Chem. Eng. Sci.* **2019**, *196*, 463–477. [[CrossRef](#)]
49. Wang, P.; Yvon, M.; Parkes, S.; Galvin, K.P. Enhancing nickel grade and recovery with counter-current washing of the concentrated bubbly-zone of a single stage REFLUX™ Flotation Cell. *Miner. Eng.* **2024**, *206*, 108506. [[CrossRef](#)]
50. Parkes, S.; Wang, P.; Galvin, K.P. Investigating the System Flotation Kinetics of Fine Chalcopyrite in a REFLUX™ Flotation Cell using a Standardised Flotation Cell Reference Method. *Miner. Eng.* **2022**, *178*, 107411. [[CrossRef](#)]

51. Boycott, A. Sedimentation of blood corpuscles. *Nature* **1920**, *104*, 532. [[CrossRef](#)]
52. Chen, J.; Chimonyo, W.; Peng, Y. Flotation behaviour in reflux flotation cell—A critical review. *Miner. Eng.* **2022**, *181*, 107519. [[CrossRef](#)]
53. Cole, M.J.; Galvin, K.P.; Dickinson, J.E. Maximizing recovery, grade and throughput in a single stage Reflux Flotation Cell. *Miner. Eng.* **2021**, *163*, 106761. [[CrossRef](#)]
54. Jiang, K. Fast Flotation in a Reflux Flotation Cell. In *Discipline of Chemical Engineering*; The University of Newcastle: Callaghan, NSW, Australia, 2017.

Disclaimer/Publisher’s Note: The statements, opinions and data contained in all publications are solely those of the individual author(s) and contributor(s) and not of MDPI and/or the editor(s). MDPI and/or the editor(s) disclaim responsibility for any injury to people or property resulting from any ideas, methods, instructions or products referred to in the content.